

Abstract. We present a fit to the spectral energy distribution of OH 127.8+0.0, a typical asymptotic giant branch star with an optically thick circumstellar dust shell. The fit to the dust spectrum is achieved using non-spherical grains consisting of metallic iron, amorphous and crystalline silicates and water ice. Previous similar attempts have not resulted in a satisfactory fit to the observed spectral energy distributions, mainly because of an apparent lack of opacity in the 3–8 μm region of the spectrum. Non-spherical metallic iron grains provide an identification for the missing source of opacity in the near-infrared. Using the derived dust composition, we have calculated spectra for a range of mass-loss rates in order to perform a consistency check by comparison with other evolved stars. The $L - [12 \mu\text{m}]$ colours of these models correctly predict the mass-loss rate of a sample of AGB stars, strengthening our conclusion that the metallic iron grains dominate the near-infrared flux. We discuss a formation mechanism for non-spherical metallic iron grains.

Key words: stars: AGB and post-AGB – circumstellar matter – dust, extinction – radiative transfer – infrared: stars

Dust and the spectral energy distribution of the OH/IR star OH 127.8+0.0: Evidence for circumstellar metallic iron*

F. Kemper¹, A. de Koter¹, L.B.F.M. Waters^{1,2}, J. Bouwman^{1**}, and A. G. G. M. Tielens^{3,4}

¹ Astronomical Institute "Anton Pannekoek", University of Amsterdam, Kruislaan 403, 1098 SJ Amsterdam, The Netherlands

² Instituut voor Sterrenkunde, Katholieke Universiteit Leuven, Celestijnenlaan 200B, B-3001 Heverlee, Belgium

³ Kapteijn Institute, University of Groningen, P.O. Box 800, 9700 AV Groningen, The Netherlands

⁴ SRON Laboratory for Space Research, P.O. Box 800, 9700 AV Groningen, The Netherlands

Received / Accepted

1. Introduction

Oxygen-rich Asymptotic Giant Branch (AGB) stars show an infrared excess on their spectral energy distribution (SED), which arises from thermal emission of dust located in a circumstellar shell. It is well established that the dust in this shell mainly consists of silicates, deduced from the clear detection of the 10 and 18 μm features. These bands are due to the Si-O bond stretching and Si-O-Si bond bending vibrations, respectively. It was noticed already some 25 years ago (Jones & Merrill 1976; Bedijn 1977) that the opacities of various types of silicates measured in the laboratory, were not high enough to explain the shape of the spectrum in the near-infrared (NIR, $3 < \lambda < 8 \mu\text{m}$). Jones & Merrill (1976) investigated the effect of pure silicates with graphite inclusions and of meteoritic rock on the shape of the SED. These materials were taken to represent silicates with various metallic inclusions, and referred to as *dirty silicates*. Radiative transfer calculations using the opacity of dirty silicates were in good agreement with the observations. Draine & Lee (1984) used laboratory measurements of limited resolution and wavelength coverage (Huffman & Stapp 1973) in which the optical constants are partly modified and expanded in wavelength regime to match the astronomical observations of interstellar and circumstellar silicates (Jones & Merrill 1976; Rogers et al. 1983). These optical constants are usually referred to as *astronomical silicate*. The exact chemical composition of this astronomical silicate is not known, nevertheless it is widely used in theoretical studies of the radiative transfer in circumstellar dust shells (e.g. Bedijn 1987; Schutte & Tielens 1989; Justtanont & Tielens 1992;

Le Sidaner & Le Bertre 1993). Recently there have been efforts to derive improved optical constants for astronomical silicates, both for lines-of-sight in the interstellar medium (ISM) and toward oxygen-rich evolved stars exclusively (Ossenkopf et al. 1992; David & Pégourié 1995; Suh 1999). These optical constants still do not provide the answer to the composition and the nature of circumstellar silicates.

The study of circumstellar dust shells in the pre-ISO era was based on low resolution spectroscopy, but with the launch of the Infrared Space Observatory (ISO) (Kessler et al. 1996), a large wavelength region, from 2–200 μm , became available for intermediate resolution spectroscopic observations ($\lambda/\Delta\lambda \gtrsim 400$). The ISO spectra of oxygen-rich evolved stars turned out to be extremely rich in solid state features. Hence, it became meaningful to attempt spectral fits using properly characterized cosmic dust analogs, rather than astronomical silicates. Demyk et al. (2000) aim to do this for OH/IR stars (i.e. AGB stars with an optically thick dust shell), but their work is not complete and parts of the spectrum are not fitted to a satisfactory level. Harwit et al. (2001) have studied the optically thin dust shell surrounding red supergiant VY CMa and are able to fit the SED, albeit after including a large overabundance of metallic iron in the dust composition.

In this study, we aim to determine the dust composition with full radiative transfer calculations using exclusively optical constants of well-defined materials measured in the laboratory, examining all astronomically relevant materials, and taking abundance constraints into account. Revealing the exact dust composition is an important step toward understanding dust formation and processing in the outflows of oxygen-rich evolved stars.

The paper is organized as follows: In Sect. 2 we discuss the spectral energy distribution arising from full radiative transfer calculations using amorphous olivine as the only dust component, and compare it to the observations. Sect. 3 discusses the dust composition and grain properties required to improve the fit to the observations. A spectral fit to OH 127.8+0.0 is presented in Sect. 4,

Send offprint requests to: F. Kemper, (ciska@science.uva.nl)

* Based on observations with ISO, an ESA project with instruments funded by ESA Member States (especially the PI countries: France, Germany, the Netherlands and the United Kingdom) and with the participation of ISAS and NASA.

** present address: Service d'Astrophysique, CEA/DSM/DAPNIA, C.E. Saclay, F-91191 Gif-sur-Yvette, France

supported by a consistency check on other AGB stars in Sect. 5. Section 6 contains a discussion of the results.

2. Modelling the circumstellar environment

In this section we describe and discuss the results from the radiative transfer calculations assuming that the dust only consists of amorphous olivine. We describe the discrepancies between the calculated and observed spectral energy distributions of AGB stars.

2.1. Model assumptions and default grid

Our approach is to calculate a set of model spectra of dust shells characteristic for both Mira and OH/IR stars, and to compare these with ISO observations. The stellar and wind parameters are the same for all models in the grid, except for the mass-loss rate which is varied from relatively low values, typical for Mira's, to relatively large values, characteristic for OH/IR stars. This leads to a variety of optical depths, which can be compared to the optical depth in the $10\ \mu\text{m}$ feature of observed spectra. A similar approach has been taken by Bedijn (1987) who also studied the appearance of the SED of AGB stars as a function of mass loss, comparing the results with IRAS observations and ground based infrared data.

We use the code MODUST to model the spectrum of the circumstellar dust shell. The radiative transfer technique applied in this code has been outlined by Kemper et al. (2001). The specification of grain properties, such as size and shape distribution, are discussed in Bouwman et al. (2000). Here, we only discuss details relevant for the presented models. The dust is assumed to be distributed in a spherical shell, with inner radius R_{in} and outer radius R_{out} , which is irradiated by a central star with $T_{\text{eff}} = 2.7 \cdot 10^3\ \text{K}$, a radius $R_{\star} = 372\ R_{\odot}$ and a luminosity $L_{\star} = 6.3 \cdot 10^3\ L_{\odot}$, thus describing a typical AGB star. The input spectrum of the central star is not simply a black body but is a characteristic mean spectrum for spectral type M9III, inferred from observations ($380\ \text{nm} \lesssim \lambda \lesssim 900\ \text{nm}$) and extended with synthetic spectra in the range $99 - 12500\ \text{nm}$ (Fluks et al. 1994). The M9III star with a $T_{\text{eff}} = 3126\ \text{K}$, emits significantly less flux at $\lambda < 1\ \mu\text{m}$ than a black body of the same temperature. Dust is efficiently heated in this wavelength region, and therefore the dust located at the inner edge of the dust shell around an M9III star would be somewhat cooler than the dust at the inner radius around a black body of $3126\ \text{K}$. This temperature difference decreases with distance from the central star. In case of an optically thin dust shell, the observed spectrum is dominated by the thermal emission of the warm dust at the inner radius. Therefore, the silicate features are somewhat stronger in case the black body is used as a central source. In case of an optically thick dust shell, there is no difference in the spectral energy distribu-

Table 1. Inner radius of the dust shell used in our initial model calculations, for different mass-loss rates, based on the work of Bedijn (1987).

$M\ (M_{\odot}\ \text{yr}^{-1})$	$R_{\text{in}}\ (R_{\star})$
5(-8)	6.05
1(-7)	6.20
2(-7)	6.37
5(-7)	6.56
1(-6)	6.91
2(-6)	7.26
5(-6)	8.23
1(-5)	9.17
2(-5)	10.2
5(-5)	12.3
1(-4)	14.3
2(-4)	17.8
5(-4)	23.5
1(-3)	29.0

tion between the two possibilities, because only the dust in the outer regions is visible for the observer.

The adopted mass-loss rates range between $5 \cdot 10^{-8}$ and $1 \cdot 10^{-3}\ M_{\odot}\ \text{yr}^{-1}$. The inner radius of the dust shell is defined by the condensation temperature of amorphous silicate, taken to be $T_{\text{cond}} = 900\ \text{K}$ (Bedijn 1987). The exact location of the inner radius is determined by the largest grains and is a function of the mass-loss rate as the dust density in the shell determines the diffuse component of the radiation field, also known as backwarming, thus constraining the temperature profile. The values for R_{in} range from 6.05 to $29\ R_{\star}$ for the smallest and largest mass loss, respectively (see Tab. 1). The outer radius is chosen to scale correspondingly to $100\ R_{\text{in}}$. This is significantly lower than what is used by others (e.g. Bedijn 1987), but higher values lead to an overestimation of the flux around $20 - 25\ \mu\text{m}$. The dust density in the shell is determined using a constant outflow velocity of $20\ \text{km s}^{-1}$, implying the density decreases as $\rho(r) \propto r^{-2}$. We used a dust/gas mass ratio of 0.01.

To obtain the absorption and scattering efficiencies we used optical constants of an amorphous olivine (MgFeSiO_4) sample measured by Dorschner et al. (1995) and assumed that the grains are spherical, such that Mie theory can be applied (see van de Hulst 1957; Bohren & Huffman 1983). The size distribution of grains was assumed to be interstellar, i.e. given by $n(a) \propto a^{-3.5}$, where a is the grain size (Mathis et al. 1977). For the circumstellar silicates we adopted a minimum and maximum size of the grains of 0.01 and $1\ \mu\text{m}$.

2.2. Problems in fitting the SED of AGB stars

Figure 1 shows a comparison of two of our predicted SEDs with the ISO spectrum of the oxygen-rich star OH

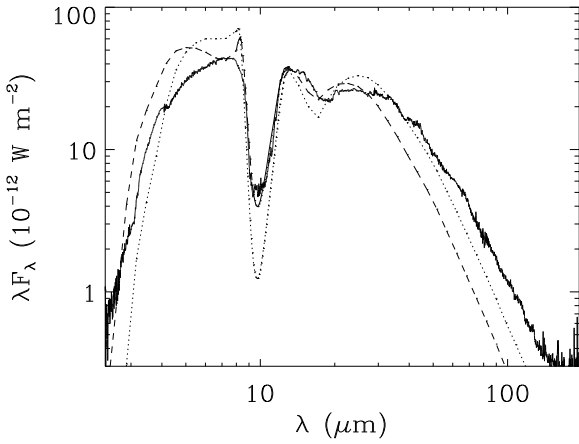


Fig. 1. ISO spectrum of OH 127.8+0.0 (solid line), together with two model spectra. The dashed line is the SED of the model with $\dot{M} = 1 \cdot 10^{-4} M_{\odot} \text{ yr}^{-1}$, and the dotted line corresponds to the model with $\dot{M} = 2 \cdot 10^{-4} M_{\odot} \text{ yr}^{-1}$. Note the discrepancies between the model fits and the observed spectrum at $\lambda = 3\text{--}8 \mu\text{m}$ region, at the peak position of the $18 \mu\text{m}$ feature and at the long wavelength part of the spectrum.

127.8+0.0 (solid line). The models with mass loss $1 \cdot 10^{-4}$ (dashed line) and $2 \cdot 10^{-4} M_{\odot} \text{ yr}^{-1}$ (dotted line) were selected. The first because it fits the $10 \mu\text{m}$ region best; the second because it gives the best overall shape of the spectrum, even though the discrepancies remain large. The poor agreement between the model spectrum and observations illustrates the problem of fitting AGB spectra. The main discrepancies are: **i)** the NIR flux is overestimated. **ii)** the shape and predicted position of the olivine resonance at $18 \mu\text{m}$ are not well reproduced, complicating the fit to the mid-infrared (MIR, $8 < \lambda < 30 \mu\text{m}$) spectrum. Specifically, we predict the center of this absorption feature at $16.3 \mu\text{m}$. **iii)** The flux in the far-infrared (FIR, $\lambda > 30 \mu\text{m}$) is underestimated, and the models show a steeper spectral slope than observed. In Sect. 3 these problems will be discussed and resolved. All three issues can be explained in terms of dust composition and grain properties.

3. Improvements to the spectral fit

3.1. Metallic iron as a source of NIR opacity

Let us first focus on the behaviour of the two predicted spectra. In both models the radial monochromatic *absorption* optical depth in the NIR is about equal to or somewhat larger than unity; in the 10 and $18 \mu\text{m}$ feature the dust medium is optically thick, while in the FIR it is optically thin. This is shown in Fig. 2, where the optical depth is given for a typical dust shell consisting of only amorphous olivine. In general, the flux at short wavelengths

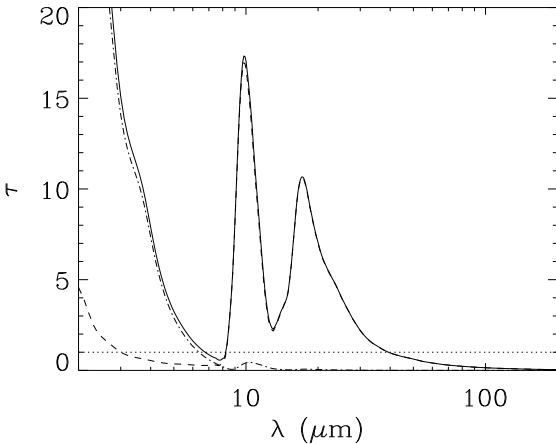


Fig. 2. Optical depth towards the central star in the dust shell of an evolved star with a gas mass-loss rate $1 \cdot 10^{-4} M_{\odot} \text{ yr}^{-1}$. The used optical constants are from amorphous olivine (Dorschner et al. 1995). $\tau = 1$ is indicated with the dotted line. The dashed line indicates absorption and the dashed-dotted line denotes scattering. The solid line represents the combined optical depth due to both effects. Note that the combined optical depth is dominated by scattering for $\lambda < 8 \mu\text{m}$ and by absorption for $\lambda > 8 \mu\text{m}$.

decreases with increasing density as a larger fraction of the thermal radiation emitted by the hottest grains suffers additional thermalization in colder regions of the dust medium. So, one way to further reduce the NIR flux is simply to increase the mass-loss rate. However, this will also increase the optical depth at 10 and $18 \mu\text{m}$, and by that will overpredict the absorption strength of these features. Thus, varying the physical parameters, such as the density distribution, the inner radius and the outer radius, will not cause a wavelength dependent effect on the optical depth. In order to resolve the NIR problem one needs to selectively increase the opacity at these wavelengths, i.e. a species is missing of which the absorption efficiency follows a *smooth* distribution – as no unidentified resonances are present – predominantly contributing in the $3\text{--}8 \mu\text{m}$ region. Using the model grid calculations to fit the optical depth at various wavelengths, we can estimate that $\tau_{\text{NIR}}/\tau_{10 \mu\text{m}} \approx 1/5$.

For chemistry and abundance reasons we considered the following dust species which could be present in oxygen-rich dust shells: metallic Fe (Ordal et al. 1988), FeO (Henning et al. 1995), SiO₂ (Gray 1963; Drummond 1936; Spitzer & Kleinman 1961; Philipp 1985; Longtin et al. 1988), Fe₃O₄ (Steyer 1974), Al₂O₃ (Koike et al. 1995; Begemann et al. 1997) and amorphous and crystalline H₂O ice (Bertie et al. 1969; Warren 1984). The mass absorption coefficients and extinction efficiencies have been determined from the optical constants. The missing source of opacity has to contribute significantly to the continuum

in the $3\text{--}8\ \mu\text{m}$ region, but should not show strong and narrow features in the $2\text{--}20\ \mu\text{m}$ region. This eliminates SiO_2 and water ice for this purpose. SiO_2 has very strong resonances at ~ 8.7 , ~ 12.4 , ~ 14.4 and $\sim 20.5\ \mu\text{m}$, while the contribution to the continuum in the $3\text{--}8\ \mu\text{m}$ region is orders of magnitude less. These sharp resonances are not observed, therefore only a small amount of SiO_2 can be present in the dust shell, which is not enough to significantly increase the NIR opacity. Water ice, both amorphous and crystalline, has features at ~ 3.1 , ~ 4.4 , ~ 6.3 and $\sim 12\ \mu\text{m}$. In between these features, the continuum is relatively weak. The ~ 3.1 micron feature is the strongest feature and is actually seen in absorption in most AGB spectra. The amount of water ice required to fit this feature explains only a negligible fraction of the NIR opacity. Fig. 3 shows the mass absorption coefficients of the remaining candidates, with broad band or continuum emission in the NIR wavelength region, calculated for both spherical and non-spherical particles. A continuous distribution of ellipsoids (CDE, see Bohren & Huffman 1983) is used to represent non-spherical grains. The strongest contribution in the $3\text{--}8\ \mu\text{m}$ region is caused by non-spherical metallic iron particles, suggesting these are a likely candidate for the missing opacity in the NIR in the spectrum of AGB stars. The mass absorption coefficients of FeO and Al_2O_3 are much lower in the NIR region, while the contribution at longer wavelengths is more significant. This rules these species out as the missing source of opacity. Fe_3O_4 does contribute in the NIR although a factor of 2 less than Fe, but shows spectral features in the $15\text{--}20\ \mu\text{m}$ region which are not observed in the spectrum. In this study we will therefore concentrate on Fe as the most likely candidate for the moving NIR opacity, because it has the highest mass absorption coefficient in the $3\text{--}8\ \mu\text{m}$ region and the most favourable spectroscopic properties.

3.2. Non-spherical grains

The shift in the peak position of the $18\ \mu\text{m}$ feature between model calculations and observations is a second problem that occurs. This can be solved using non-spherical amorphous olivine grains. The difference between the mass absorption coefficients of spherical and non-spherical olivine grains is clearly shown in Fig. 2 of the work by Demyk et al. (2000). In particular the shape of the $18\ \mu\text{m}$ feature is much affected and the peak position shifts to a somewhat longer wavelength for non-spherical grains. However, Demyk et al. (2000) did not use these non-spherical particles in their radiative transfer calculations of optically thick dust shells.

A continuous distribution of ellipsoids (CDE) may better approximate the actual variety of grain shapes that is present in the outflow of evolved stars. The optical properties are dependent on the shape, which is for example apparent in a shift of the peak position of spectral features. Shape effects are most prominent for conducting mate-

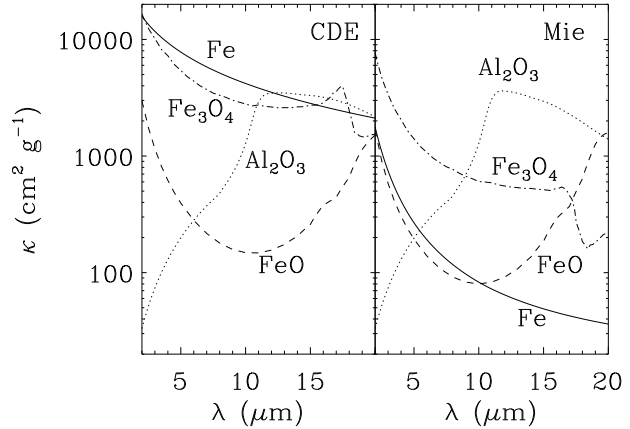


Fig. 3. Mass absorption coefficients κ ($\text{cm}^2\ \text{g}^{-1}$) as a function of wavelength for different species contributing in the NIR. The left panel shows the calculations for a continuous distribution of ellipsoids (CDE) which supposedly represents non-spherical particles, and the right panel shows the Mie calculations, used for spherical particles. The labels indicate the mass absorption coefficient curves for the considered species. Note the large differences between the mass absorption coefficients for CDE and Mie calculations in case of metallic iron and Fe_3O_4 , caused by their highly conductive nature.

rials. Strictly speaking, the CDE approximation is only valid in the Rayleigh limit, where the size of the particles is at least a factor of ~ 20 smaller than the wavelength. As we are using CDE calculations to solve problems with the $18\ \mu\text{m}$ feature and our maximum grain size used is $1.0\ \mu\text{m}$, this condition is not violated. The result that metallic iron in CDE accounts for the missing NIR opacity, is also consistent with the Rayleigh limit, because the metallic iron grains are probably incorporated in the silicate grains (see Sect. 6) and therefore have sizes significantly smaller than $1.0\ \mu\text{m}$. For an elaborate description of resonances and the absorption characteristics of non-spherical particles the reader is referred to Bohren & Huffman (1983).

3.3. Water ice features in the far-infrared

The improved fit to the NIR part of the SED leads to a redistribution of the radiation such that the flux in the NIR is suppressed and FIR flux levels are increased. Additional improvement of the FIR flux might be achieved by adjusting the outer radius of the dust shell, where cold dust – optically thin in the FIR – contributes. The remaining discrepancy between the observed and modelled flux levels at the long wavelength side can probably be overcome by water ice as an additional dust component. The presence of the 3 , 43 and $60\ \mu\text{m}$ features in most OH/IR stars implies that crystalline water ice is an important

dust component (Sylvester et al. 1999). The $3\ \mu\text{m}$ feature is seen in absorption (see also Sect. 3.1). In addition to the 43 and $60\ \mu\text{m}$ emission features, crystalline water ice also has an intrinsically strong underlying continuum $> 30\ \mu\text{m}$ which contributes to the FIR emission in the SED.

4. Results for OH 127.8+0.0

4.1. Stellar parameters and radiative transfer modelling

We have constructed a model representative for AGB stars, with the intention to fit the spectrum of OH 127.8+0.0, a high mass-loss rate AGB star. The input spectrum at the inner radius is that of a star with spectral type M9III (Fluks et al. 1994), and a radius of $372\ R_{\odot}$. The density distribution and total mass of the dust shell are determined by the velocity profile and the inner and outer radii. The outflow velocity was again set to $20\ \text{km s}^{-1}$, implying a density distribution $\propto r^{-2}$. In reality the wind probably accelerates while dust is being formed in the inner regions, until it reaches the terminal velocity. However, the dust shell is very optically thick in the NIR, where the warm dust in the inner regions most effectively radiates, implying that density variations in the inner parts – well inside the $\tau = 1$ surface – of the dust shell do not affect the emerging SED. Therefore it is impossible to further constrain the velocity profile and the inner radius; we chose the latter to be consistent with a condensation temperature of $\sim 900\ \text{K}$, using $R_{\text{in}} = 14.3\ R_{\ast}$ ($3.7 \cdot 10^{14}\ \text{cm}$). This temperature corresponds to the condensation temperature of amorphous silicates, but crystalline silicates and metallic iron condense at higher temperatures (Gail & Sedlmayr 1999). We performed test calculations in which we varied the inner radius and did not see a difference in the resulting SED. It is possible to determine the outer radius, found to be at $R_{\text{out}} = 5000\ R_{\ast}$ ($1.3 \cdot 10^{17}\ \text{cm}$), with an accuracy of 15%, by fitting the slope in the FIR. By fitting the optical depth of the $10\ \mu\text{m}$ silicate feature, the dust mass-loss rate was found to be $7(\pm 1) \cdot 10^{-7} M_{\odot}\ \text{yr}^{-1}$, which translates in a gas mass-loss rate of $7(\pm 1) \cdot 10^{-5} M_{\odot}\ \text{yr}^{-1}$, assuming a dust/gas ratio 0.01. Together with R_{out} this parameter determines the total dust mass in the shell surrounding OH 127.8+0.0 and sets it to be $1.4 \cdot 10^{-3} M_{\odot}$.

By scaling the SED to the observations, we find that the distance toward OH 127.8+0.0 is 1800 (± 50) pc, which assumes the stellar luminosity is $6300\ L_{\odot}$. This is significantly smaller than results using the phase lag of the 1612 MHz OH maser in combination with imaging. Herman & Habing (1985) find a distance of $6.98\ \text{kpc}$, and Bowers & Johnston (1990) report $6.21 \pm 1.0\ \text{kpc}$, using the phase lag determination of Herman & Habing (1985). Such a large distance consequently leads to a very high luminosity ($2.6 \cdot 10^5\ L_{\odot}$), more typical for red supergiants than OH/IR stars. Other studies result in distances of $5.6\ \text{kpc}$ (Engels et al. 1986) and $2.8\ \text{kpc}$ (Heske et al. 1990).

4.1.1. Dust properties

We find that the dust shell consists of the following dust components: amorphous olivine (80% by mass), forsterite (3%), enstatite (3%), metallic iron (4%) and crystalline water ice (10%, $T_{\text{cond}} = 150\ \text{K}$), based on the assumption that all dust species are present in separate grain populations. The crystalline silicates forsterite and enstatite are identified in the spectra of AGB stars (Sylvester et al. 1999), and their relative mass fraction is assumed to be 3% each, a typical value for AGB stars (Kemper et al. 2001). We did not attempt to fit the actual mass fraction taken by enstatite and forsterite, which is subject to further study (Kemper et al., in prep.). The overall shape of the SED is not affected by assuming a degree of crystallinity of 3%, since aside from the sharp resonances in the MIR, the opacities of amorphous and crystalline silicates are comparable. All dust is found to be present in non-spherical (CDE) grains. The adopted optical constants of crystalline and amorphous silicates are provided by Dorschner et al. (1995), Jäger et al. (1998) and Koike (priv.comm.). For crystalline water ice we used the optical constants derived by Bertie et al. (1969) and Warren (1984); the optical constants of metallic iron are taken from Ordal et al. (1988).

Fig. 4 shows the fit to OH 127.8+0.0. The ISO spectroscopy is taken from Sylvester et al. (1999) and the 60 and $100\ \mu\text{m}$ photometry originates from the IRAS Point Source Catalog. Additional observations with the James Clerk Maxwell Telescope (JCMT) have been performed to obtain the 450 and $850\ \mu\text{m}$ photometry points (Kemper et al., in prep.). It is clear that if 4% of the total dust mass is contained in non-spherical metallic iron grains, the NIR problem is solved. This is consistent with the average interstellar Fe and Si abundances (Snow & Witt 1996) that allow a mass fraction of 15% in the form of metallic iron, with respect to amorphous olivine.

In order to fit the FIR part of the SED, it is required to include a significant fraction of water ice in the dust shell (10%) for which a condensation temperature of $150\ \text{K}$ is assumed. This is consistent with the mass fraction contained in water ice in the oxygen-rich dust shell of post-AGB star HD 161796 (Hoogzaad et al., in prep.).

4.2. Comparison with astronomical silicate

The derived total dust extinction toward OH 127.8+0.0 can be compared with astronomical and laboratory measurements. The extinction efficiency Q_{ext} of the individual dust species assuming CDE have been added proportionately and the resulting total Q_{ext} is plotted in Fig. 5. Note that all curves are normalised to the strength of the $10\ \mu\text{m}$ feature to emphasize the differences in the NIR region. To provide some quantitative insight, Tab. 2 presents the extinction efficiencies at $7\ \mu\text{m}$ and at $18\ \mu\text{m}$ with respect to the extinction efficiencies at $10\ \mu\text{m}$. The long-dashed

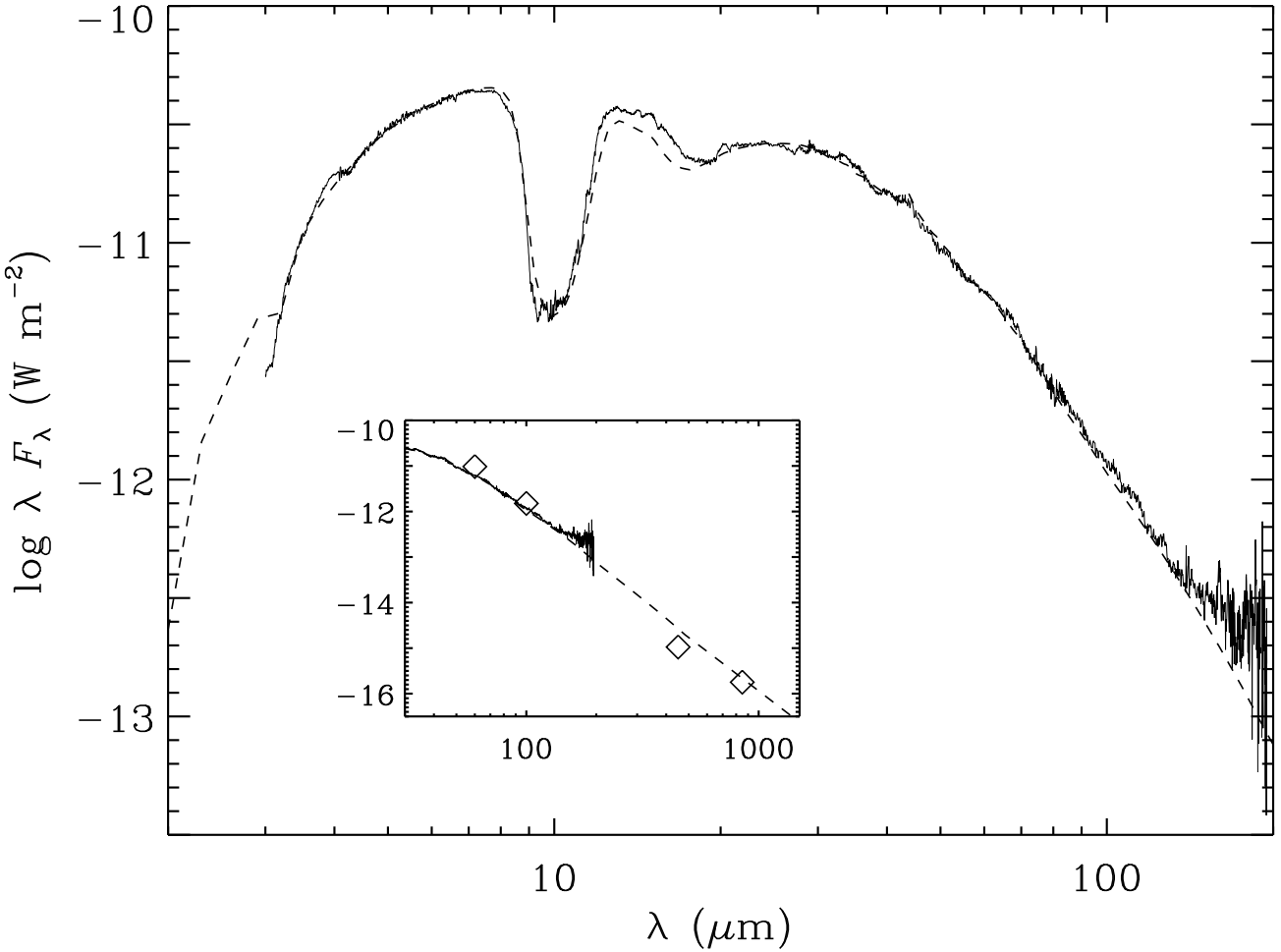


Fig. 4. The large panel shows the fit (dashed line) to the ISO spectrum of OH 127.8+0.0 (solid line). In the inset, the same fit is presented for the 30 – 1500 μm wavelength range. The diamonds indicate the IRAS 60 and 100 μm and JCMT SCUBA 450 and 850 μm photometry points. The error bars on the measurements are smaller than the size of the symbols. A mass fraction of 4% of metallic iron was included in the dust. See Sect. 4 for a description of the model parameters and the dust composition.

line shows the extinction efficiency for a synthesized pure amorphous olivine (Dorschner et al. 1995). One can see easily that for this species the NIR extinction is very small compared to the efficiency at 10 μm . Also shown in the figure are astronomical silicates derived from ISM lines-of-sight (Draine & Lee 1984; Ossenkopf et al. 1992) and toward late-type stars (Ossenkopf et al. 1992; David & Pégourié 1995; Suh 1999). Only the work of Ossenkopf et al. (1992) assumes non-spherical grains and uses CDE as a representation of grain shapes. The other efficiencies are calculated using Mie scattering for spherical particles.

The optical constants derived by David & Pégourié (1995) from G and M supergiants, closely resemble the synthetic olivine in the NIR region. The 10 μm resonance is much narrower, while the efficiency at longer wavelengths is again significantly less compared to our result.

All in all, the David & Pégourié result gives the poorest match to our findings. Suh (1999) has derived the optical constants from AGB stars and splits them into two different types: *warm* and *cool* silicates, representative for low and high mass-loss rate AGB stars respectively. This dichotomy assumes a difference in composition of the bulk material. In Fig. 5, we present the efficiency for cool dust as this is most appropriate for the optically thick dust shell modeled in this work. The Suh result compares reasonably well with our finding, though the NIR efficiency is less and the 18 μm efficiency is somewhat larger. Ossenkopf et al. (1992) distinguish between interstellar *O-rich* silicates (olivines) and circumstellar *O-deficient* silicates (pyroxenes), without discriminating between optically thin and thick dust shells. Shown in Fig. 5 are the *O-deficient* silicates which represent the most meaningful comparison with our model. In the NIR the Ossenkopf et

Table 2. Relative extinction efficiencies at 7 and 18 μm compared to the extinction efficiency at 10 μm , in addition to Fig. 5.

optical constants	$Q_{\text{ext}}(7 \mu\text{m})$	$Q_{\text{ext}}(18 \mu\text{m})$	ref.
	$Q_{\text{ext}}(10 \mu\text{m})$	$Q_{\text{ext}}(10 \mu\text{m})$	
OH 127.8+0.0	0.22	0.67	
O-rich silicate	0.15	0.61	Ossenkopf et al. (1992)
O-deficient silicate	0.12	0.47	Ossenkopf et al. (1992)
astronomical silicate	0.087	0.39	Draine & Lee (1984)
warm silicate	0.085	0.37	Suh (1999)
cold silicate	0.080	0.78	Suh (1999)
astronomical silicate	0.041	0.12	David & Pégourié (1995)
amorphous olivine	0.017	0.68	Dorschner et al. (1995)

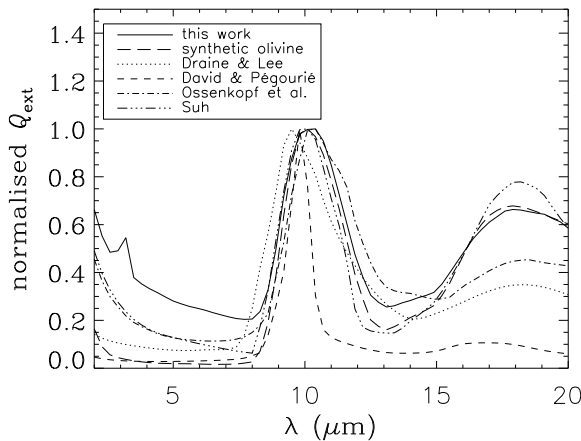


Fig. 5. Comparison of the extinction efficiency Q_{ext} for the composition found for the circumstellar dust shell of OH 127.8+0.0 (this work), compared with the Q_{ext} of synthesized amorphous olivine (Dorschner et al. 1995), and the Q_{ext} for several different astronomical silicates (Draine & Lee 1984; Ossenkopf et al. 1992; David & Pégourié 1995; Suh 1999). All extinction efficiencies are normalised on the 10 μm peak strength to allow comparison of the NIR extinction.

al. result compares best with our efficiencies, although they still find a lower Q_{ext} . In the 18 μm region their efficiencies also fall below our work.

So, the dust composition determined in this paper provides the only result that produces sufficient NIR flux. One should note, however, that our results are of course sensitively dependent on the metallic iron content of the AGB star, and may vary from source to source, whereas other studies tried to derive mean values for a sample of stars.

5. A consistency check

The SED of OH 127.8+0.0 is typical for high mass-loss rate AGB stars, which justifies the calculation of a series of models for varying mass-loss rates, while the dust compo-

sition and other physical parameters were kept the same. Gail & Sedlmayr (1999) show that metallic iron and silicates condense simultaneously in the stellar outflow, suggesting that the relative mass fraction of iron compared to the silicates remains constant. We allowed the inner radius to change in order to satisfy the constraint that the condensation temperature $T_{\text{cond}} = 900$ K.

Using the SEDs predicted by the model, the infrared colours in different stages of the mass-loss evolution on the AGB can be determined. For example, the relation between the $K - [12 \mu\text{m}]$ colour or $K - L$ colour and the optical depth is a useful diagnostic tool to determine the mass-loss rate of an AGB star (Le Sidaner & Le Bertre 1996; Le Bertre & Winters 1998). We searched for the presence of a relation between the $L - [12 \mu\text{m}]$ colour index and the mass-loss rate, since the $L - [12 \mu\text{m}]$ colour can be determined from ISO SWS spectroscopy directly. For the L-band (3.6 μm) we use the transmission profile provided by Bessell & Brett (1988); for the magnitude calibration an absolute flux density for zero magnitude of 277 Jy was used (Koornneef 1983). The standard IRAS transmission profile and calibration are used to determine the magnitude in the 12 μm band. The calculated absolute magnitudes and the colour indices are summarized in Table 3.

Fig. 6 shows the correlation between the $L - [12 \mu\text{m}]$ colour and the mass-loss rate derived from our model calculations. In addition, we have included the mass-loss rates and infrared colours of five stars taken from the sample of Sylvester et al. (1999). The $L - [12 \mu\text{m}]$ colour is obtained directly from the ISO spectroscopy. We can see that within the accuracy of the mass-loss rate determinations, a metallic iron fraction of 4% gives reasonable results, thus providing a consistency check that adding metallic iron can explain the infrared colours of other AGB stars as well. From the figure it becomes also clear that modifications of the iron mass fraction probably improves the result. To determine the iron mass fraction, detailed full radiative transfer calculations are necessary.

Table 3. Absolute magnitudes and infrared colour index as a function of mass-loss rate, for modelled SEDs with 4% of the dust mass contained in non-spherical metallic iron grains.

\dot{M} (M_{\odot} yr $^{-1}$)	$M_{[12]}$	M_L	$L - [12]$
4(-8)	-8.8	-7.4	1.4
7(-8)	-9.0	-7.4	1.6
1(-7)	-9.1	-7.4	1.7
2(-7)	-9.4	-7.5	2.0
4(-7)	-9.9	-7.5	2.4
7(-7)	-10.3	-7.5	2.8
1(-6)	-10.6	-7.6	3.0
2(-6)	-11.0	-7.7	3.3
4(-6)	-11.5	-7.9	3.6
7(-6)	-11.6	-7.9	3.7
1(-5)	-11.7	-8.0	3.7
2(-5)	-11.9	-7.8	4.1
4(-5)	-11.9	-7.4	4.4
7(-5)	-11.9	-6.8	5.1
1(-4)	-11.8	-6.3	5.5
2(-4)	-11.6	-4.9	6.7
4(-4)	-11.2	-3.2	8.0
7(-4)	-10.7	-1.7	9.0
1(-3)	-10.1	-0.7	9.4

6. Discussion

The results presented in this work provide the first sound identification of metallic iron in the circumstellar dust shell around AGB stars, without violating abundance constraints. Demyk et al. (2000) have tried to include metallic iron in their model calculations of evolved stars, but because they did not consider non-spherical grains, metallic iron could not be abundant enough to account for the missing NIR opacity. Harwit et al. (2001) have concluded that metallic iron is necessary to fit the spectrum of VY CMa, although all Fe-atoms should be incorporated in metallic iron, implying that the amorphous silicate is completely Mg-rich, and even then a large overabundance is required.

From meteoritic and theoretical studies it is known that metallic iron can condense in a cooling gas of solar composition (e.g. Grossman & Larimer 1974; Lewis & Ney 1979; Kozasa & Hasegawa 1988). In that case, metallic iron forms almost simultaneously with silicates, since its condensation temperature is only 50 – 100 K below that of silicates. In an oxygen-rich chemistry, metallic iron is stable above 700 K. Below that temperature it will react to form FeS and/or FeO (Jones 1990).

An alternative is that it will remain metallic because it is protected from the oxidizing environment by inclusion in a grain. This can be achieved through the formation of *iron islands* on the surface of silicate grains (Gail & Sedlmayr 1999). During the formation process of silicates, Fe-atoms in the lattice will be replaced by the thermodynamically more favourable Mg. The Fe-atoms will migrate

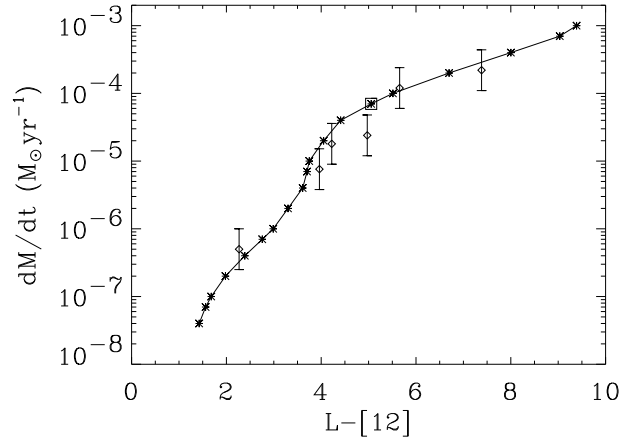


Fig. 6. The mass loss rate of oxygen-rich AGB stars as a function of the $L - [12 \mu\text{m}]$ colour index, arising from radiative transfer calculations, indicated with the asterisks. The fit parameters of OH 127.8+0.0 are indicated with a square. The diamonds represent the objects from the sample of Sylvester et al. (1999) with error bars on the mass-loss rate. The gas/dust ratio is assumed to be 100. With increasing mass-loss rates these are: *o* Cet, WX Psc, CRL 2199, OH 104.9+2.4, OH 26.5+0.6 and OH 32.8-0.3. The mass-loss rate of *o* Cet is taken from Loup et al. (1993).

to the surface of the grain to form *iron islands* and stimulate the condensation of additional Fe-atoms, to continue the growth of the islands. Gail & Sedlmayr (1999) suggest that the islands will eventually be covered by younger silicate layers, thus creating silicate grains with platelet shaped, i.e. non-spherical, metallic iron inclusions. These inclusions greatly increase the opacity of the grains in the NIR region. The model calculations presented in this work use separate grain populations, rather than metallic iron inclusions in silicate grains, but still provide an idea of the mass fraction contained in the iron inclusions. This result, together with the inclusion of crystalline water ice and the use of CDE for all grain shapes provide an important step in disentangling the dust composition of the circumstellar shell of AGB stars. No exotic assumptions were required to match the spectrum. A spherical outflow of material at constant velocity suffices to produce a good fit to the SED if chemical and shape properties of the grains are treated in sufficient detail.

The presence and formation of metallic iron in astrophysical environments has been subject to many studies in the past (Jones 1990, and references herein). Studies of the interstellar extinction toward the galactic centre (GC) revealed a discrepancy in the 3–8 μm region with the standard dirty silicate opacity (Lutz 1999; Lutz et al. 1996). Of course, this is an ISM line-of-sight, implying that amorphous carbon is an important dust component. On the other hand, the opacity contribution of amorphous

carbon is already included in the optical constants of the dirty silicate, i.e. a graphite-silicate mixture. Thus also in this case, non-spherical metallic iron grains might explain the missing opacity in the NIR region. In addition, it is known that *superparamagnetic* inclusions, such as metallic iron, in elongated silicate grains can cause these grains to align when a magnetic field is present (Mathis 1986). The alignment of silicate grains explains the polarization of starlight passing through the interstellar medium, a suggestion first made by Spitzer & Tukey (1951).

This theory appears to be supported by studies of interplanetary dust grains, which are collected by aircraft in the upper atmosphere of the Earth. Some of the collected particles are believed to be very pristine and probably even from interstellar origin, rather than being reprocessed during the formation of the solar system. These pristine particles consist of an amorphous matrix material with metal inclusions, and are referred to as GEMs (glasses with embedded metal and sulphides). Metallic iron inclusions are quite common in these supposedly interstellar grains (Bradley 1994; Martin 1995). Whether these grains really originate from the outflows of evolved stars remains subject to speculation at this moment.

Acknowledgements. FK, AdK, LBFMW and JB acknowledge financial support from NWO Pionier grant 616-78-333. We gratefully acknowledge support from NWO Spinoza grant 08-0 to E.P.J. van den Heuvel. The James Clerk Maxwell Telescope is operated on behalf of the Particle Physics and Astronomy Research Council of the United Kingdom, the Netherlands Organisation for Scientific Research and the National Research Council of Canada.

References

- Bedijn, P. J. 1977, PhD thesis, Leiden University
 —. 1987, A&A, 186, 136
- Begemann, B., Dorschner, J., Henning, T., et al. 1997, ApJ, 476, 199
- Bertie, J. E., Labb  , H. J., & Whalley, E. 1969, J. Chem. Phys., 50, 4501
- Bessell, M. S. & Brett, J. M. 1988, PASP, 100, 1134
- Bohren, C. F. & Huffman, D. R. 1983, *Absorption and scattering of light by small particles* (New York: Wiley)
- Bouwman, J., de Koter, A., van den Ancker, M. E., & Waters, L. B. F. M. 2000, A&A, 360, 213
- Bowers, P. F. & Johnston, K. J. 1990, ApJ, 354, 676
- Bradley, J. P. 1994, Science, 265, 925
- David, P. & P  gouri  , B. 1995, A&A, 293, 833
- Demyk, K., Dartois, E., Wiesemeyer, H., Jones, A. P., & d'Hendecourt, L. 2000, A&A, 364, 170
- Dorschner, J., Begemann, B., Henning, T., J  ger, C., & Mutschke, H. 1995, A&A, 300, 503
- Draine, B. T. & Lee, H. M. 1984, ApJ, 285, 89
- Drummond, D. G. 1936, Proc. Roy. Soc. (London)-Series A, 153, 328
- Engels, D., Schmid-Burgk, J., & Walmsley, C. M. 1986, A&A, 167, 129
- Fluks, M. A., Plez, B., Th  , P. S., et al. 1994, A&A, 105, 311
- Gail, H.-P. & Sedlmayr, E. 1999, A&A, 347, 594
- Gray, D. C. 1963, American Institute of Physics Handbook, 2nd edn. (New York: McGraw-Hill)
- Grossman, L. & Larimer, J. W. 1974, Rev. Geophys. Space Phys., 12, 71
- Harwit, M., Malfait, K., Decin, L., et al. 2001, ApJ, 557, 844
- Henning, T., Begemann, B., Mutschke, H., & Dorschner, J. 1995, A&AS, 112, 143
- Herman, J. & Habing, H. J. 1985, A&AS, 59, 523
- Heske, A., Habing, H. J., Forveille, T., Omont, A., & van der Veen, W. E. C. J. 1990, A&A, 239, 173
- Huffman, D. R. & Stapp, J. L. 1973, in IAU Symp. 52: Interstellar Dust and Related Topics, 297
- J  ger, C., Molster, F. J., Dorschner, J., et al. 1998, A&A, 339, 904
- Jones, A. P. 1990, MNRAS, 245, 331
- Jones, T. W. & Merrill, K. M. 1976, ApJ, 209, 509
- Justtanont, K. & Tielens, A. G. G. M. 1992, ApJ, 389, 400
- Kemper, F., Waters, L. B. F. M., de Koter, A., & Tielens, A. G. G. M. 2001, A&A, 369, 132
- Kessler, M. F., Steinz, J. A., Anderegg, M. E., et al. 1996, A&A, 315, L27
- Koike, C., Kaito, C., Yamamoto, T., et al. 1995, Icarus, 114, 203
- Koornneef, J. 1983, A&A, 128, 84
- Kozasa, T. & Hasegawa, H. 1988, Icarus, 73, 180
- Le Bertre, T. & Winters, J. M. 1998, A&A, 334, 173
- Le Sidaner, P. & Le Bertre, T. 1993, A&A, 278, 167
 —. 1996, A&A, 314, 896
- Lewis, J. S. & Ney, E. P. 1979, ApJ, 234, 154
- Longtin, D. R., Shettle, E. P., Hummel, J. R., & Pryce, J. D. 1988, A Wind Dependent Desert Aerosol Model: Radiative Properties, Tech. Rep. AFGL-TR-88-0112, Air Force Geophysics Laboratory, Hanscom AFB, MA
- Loup, C., Forveille, T., Omont, A., & Paul, J. F. 1993, A&AS, 99, 291
- Lutz, D. 1999, in Proceedings of the Conference "The Universe as seen by ISO", ESA SP-427, 623-626
- Lutz, D., Feuchtgruber, H., Genzel, R., et al. 1996, A&A, 315, L269
- Martin, P. G. 1995, ApJ, 445, L63
- Mathis, J. S. 1986, ApJ, 308, 281
- Mathis, J. S., Rumpl, W., & Nordsieck, K. H. 1977, ApJ, 217, 425
- Ordal, M. A., Bell, R. J., Alexander, R. W., Newquist, L. A., & Querry, M. R. 1988, Applied Optics, 27, 1203
- Ossenkopf, V., Henning, T., & Mathis, J. S. 1992, A&A, 261, 567
- Philipp, H. R. 1985, *Handbook of Optical Constants of Solids*, ed. E. D. Palik (Orlando, FL: Academic Press,

- Inc.), 719–747
- Rogers, C., Martin, P. G., & Crabtree, D. R. 1983, *ApJ*, 272, 175
- Schutte, W. A. & Tielens, A. G. G. M. 1989, *ApJ*, 343, 369
- Snow, T. P. & Witt, A. N. 1996, *ApJ*, 468, L65
- Spitzer, L. & Tukey, J. W. 1951, *ApJ*, 114, 187
- Spitzer, W. G. & Kleinman, D. A. 1961, *Phys. Rev.*, 121, 1324
- Steyer, T. R. 1974, PhD thesis, University of Arizona
- Suh, K.-W. 1999, *MNRAS*, 304, 389
- Sylvester, R. J., Kemper, F., Barlow, M. J., et al. 1999, *A&A*, 352, 587
- van de Hulst, H. C. 1957, *Light Scattering by Small Particles* (New York: John Wiley & Sons)
- Warren, S. G. 1984, *Applied Optics*, 23, 1206